# A nicking enzyme-assisted allosteric strategy for self-resetting DNA switching circuits

(Supplementary Information)

Haoliang Wang,[a] Xiaokang Zhang,[b] Yuan Liu,[b] Shihua Zhou*[a]

a Key Laboratory of Advanced Design and Intelligent Computing, Ministry of Education, School of Software Engineering, Dalian University, Dalian 116622, China. Email: wanghaoliang715@gmail.com, zhoushihua@dlu.edu.cn
b School of Computer Science and Technology, Dalian University of Technology, Dalian 116024, China. Email: xiaokangzhangdl@gmail.com, liuyuan.dlut@gmail.com.

## Contents

**Table S1. DNA sequence**

| Name | Sequences (from 5′ to 3′) | Length (nt) |
|---|---|---|
| A | FAM-TTGCAGTGTGTCAGTTTTCTTGTAGTCCTCATAC | 34 |
| B | GTCAGTCTTCAGTCAGTTTTGCAGTGTCGTCATT-BHQ1 | 34 |
| C | CTGACTGAAGACTGACTTTTGTATGAGGACTACAAG | 36 |
| D | CTGACACACTGCGATCACTGACGACACTGC | 30 |
| D-7 | ACTGACACACTGCCGATCACCTGACGACACTGCC | 34 |
| D-8 | GACTGACACACTGCCTGATCACACTGACGACACTGCCA | 38 |
| I1 | TGTCGTCAGTCATCGCAGAGTCACTAGATCAC | 32 |
| O1 | TCGCAGTAGTCACTAGATCAC-ROX | 21 |
| R1 | BHQ2-GTGATCTAGTGACTACTGCGATGAC | 25 |
| I2 | TGTCGTCACTTCAGGCAGAGTCACTAGATCAC | 32 |
| D2 | CTGACACACTGCCTGTAGTGACGACACTGC | 30 |
| O2 | GCAGAGTCACTAGATCAC-FAM | 18 |
| R2 | BHQ1-GTGATCTAGTGACTCTGCCTGAAG | 24 |
| I3 | TGTCGTCAGCTTTCGCAGAGTCACTAGATCAC | 32 |
| D3 | CTGACACACTGCGAATGCTGACGACACTGC | 30 |

| | | |
|---|---|---|
| H | GCAGAGTCACTAGATCACACAG | 22 |
| K | CTCACAGATACACGTTACAG-FAM | 20 |
| G1 | BHQ1-CTGTAACGTGTATCTGTGAGACTGTGTGATCTAGTGACTCTGCGAAAGC | 49 |
| P | AGTCAGTGCTAGGAGGTTCA-ROX | 20 |
| G2 | BHQ2-TGAACCTCCTAGCACTGACTACTGTGTGATCTAGTGACTCTGCGAAAGC | 49 |
| F3 | ACAGTCTCACAGATACACGTTACAG | 25 |
| F4 | ACAGTAGTCAGTGCTAGGAGGTTCA | 25 |
| F | ACTCACAACACCAGATTCAG-ROX | 20 |
| G3 | BHQ2-CTGAATCTGGTGTTGTGAGTACTGTGTGATCTAGTGACTCTGCGATGAC | 49 |
| G4 | BHQ2-CTGAATCTGGTGTTGTGAGTACTGTGTGATCTAGTGACTCTGCCTGAAG | 49 |
| F1 | ACAGTACTCACAACACCAGATTCAG | 25 |
| OA | ACTCACAACACCATCTTCAGGAACTCACTCTACCACAT | 38 |
| G5 | TCCTGAAGATGGTGTTGTGAGTCTGTGTGATCTAGTGACTCTGCCTGAAG | 50 |
| FA | ACAGACTCACAACACCATCTTCAGGA | 26 |
| OB | CACTACAACACCAGATACACTCAGTCTCAGTCATCAACAGTACC | 44 |
| G6 | ACTGAGTGTATCTGGTGTTGTAGTGGTACGTGATCTAGTGACTCTGCCTGAAG | 53 |

| | | |
|---|---|---|
| FB | GTACCACTACAACACCAGATACACTCAGT | 29 |
| W | GCAGAGTCACTAGATCACGTAC | 22 |
| OC | AGACAGTCCTTGCAGTACACTCAGTCTCAGTCATCA ACAGTACC | 44 |
| G8 | ACTGAGTGTACTGCAAGGACTGTCTCTGTGTGATCTA GTGACTCTGCGAAAGC | 53 |
| FC | ACAGAGACAGTCCTTGCAGTACACTCAGT | 29 |
| OD | CTCACAGATACACGGAACAGTCTACAGTCTTACAGA TGC | 39 |
| G7 | CTGTTCCGTGTATCTGTGAGCTGTGTGATCTAGTGAC TCTGCGAAAGC | 48 |
| FD | ACAGCTCACAGATACACGGAACAG | 24 |
| AW | GAACTCACTCTACCACATGAAC | 22 |
| AO | GTCTACAGTCTTACAGATGC-FAM | 20 |
| AD | BHQ1- GCATCTGTAAGACTGTAGACTGTTCATGTGGTA GAGTGAGTTCCTGAAG | 49 |
| OR | GTCTCAGTCATCAACAGTACC-ROX | 21 |
| OD | BHQ2-GGTACTGTTGATGACTGAGACTGAGTG | 27 |
| I4 | TGTCGTCAGTTGTCGCAGAGTCACTAGATCAC | 32 |
| D4 | CTGACACACTGCGACTAGTGACGACACTGC | 30 |
| G9 | CTGTTCCGTGTATCTGTGAGCTGTGTGATCTAGTGAC TCTGCGACAAC | 48 |
| G10 | ACTGAGTGTATCTGGTGTGTTAGTGTGTACGTGATCT AGTGACTCTGCGACAAC | 53 |

| | | |
|---|---|---|
| L | GCAGAGTCACTAGATCACGTAC | 22 |
| OE | ACTCACAACACCATCACTACGAACTCACTCTACCAC AT | 38 |
| G11 | TCGTAGTGATGGTGTTGTGAGTCTGTGTGATCTAGTG ACTCTGCCTGAAG | 50 |
| FE | ACAGACTCACAACACCATCACTACGA | 26 |
| YD | BHQ2-ATGTGGTAGAGTGAGTTCGTAGTG | 24 |
| YO | GAACTCACTCTACCACAT-ROX | 18 |

## S2. Nicking enzyme-assisted allosteric strategy

## PAGE analysis of nicking enzyme-assisted allosteric strategy

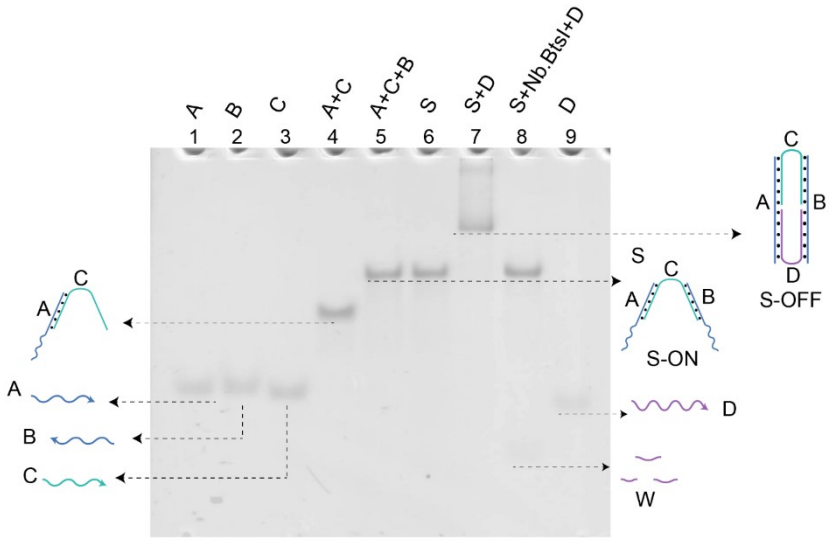


Figure S1. PAGE analysis of the nicking enzyme-assisted allosteric strategy. The input and substrate of each lane are marked at the top of the gel. ([A] = [B] = [C] = [S] = [D] = 1 μM, Nb.BtsI = 4 U).

In order to demonstrate the feasibility of the nicking enzyme-assisted allosteric strategy, we performed a polyacrylamide gel electrophoresis experiment, as shown in Figure S1. Lanes 1, 2, 3, and 9 are single strands A, B, C, and D, respectively. In lane 4, strand A reacted with strand C to form structure AC. Similarly, in lane 5, strands A, B, and C formed structure S. Compared with lane 5, in lane 6, structure S was formed by annealing strands A, B, and C. The consistency of the bands in lane 5 and lane 6 demonstrated the formation of the structure S. In lane 7, the fuel strand D induced the conformational changes from the initial “S-ON” state to the “S-OFF” state. However,

in lane 8, the presence of Nb.BtsI led to conformational changes from the initial "S-ON" state to the "S-OFF" state, followed by an automatic reset to the "S-ON" state, and the fuel strand D was cleaved into waste W.

## The Optimum number of bases for the allosteric strategy

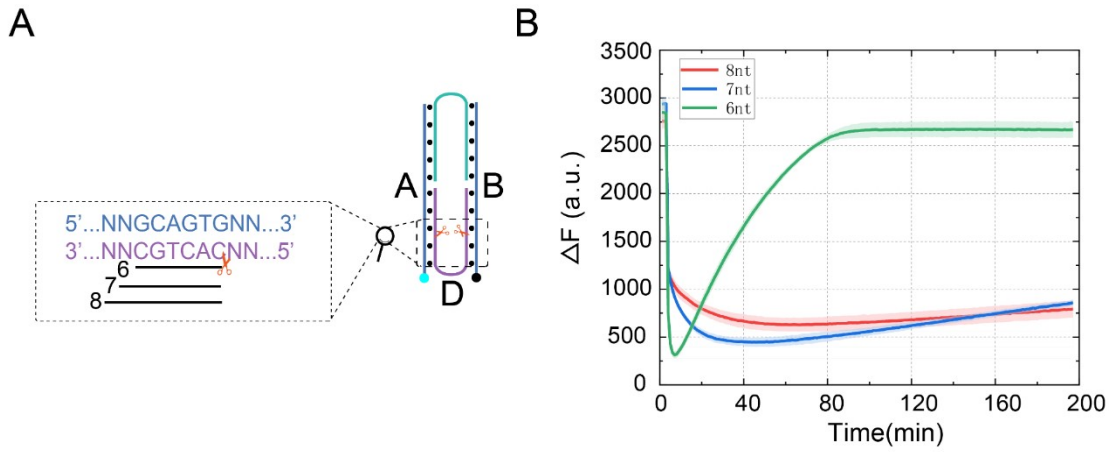


Figure S2. (A) Diagram of different base numbers in the strand D recognition domain. (B) Fluorescence analysis of self-resetting allostery strategy with different base numbers in the strand D recognition domain. The fluorescence values were averaged across the three experiments.

In order to ensure that strand D could be automatically detached from structure S after being cleaved and the structure could be restored to the initial state, we investigated the number of bases in strand D after being cleaved by the enzyme Nb.BtsI. As shown in Figure S2A, under the condition of ensuring the integrity of the recognition domain of enzyme Nb.BtsI, we selected base numbers of 6nt,7nt, and 8nt for experimental exploration. As shown in Figure S2B, we observed that when the number of bases was 8 nt and 7 nt, strand D remained connected to structure S even after being cleaved, which restricted the restoration of the structure to its initial state (red and blue curves). When the number of bases of strand D was 6nt after being cleaved, the combination of strand D and structure S was weakest, allowing for restoration to the initial state (green curve). Therefore, we selected 6 nt as the optimal number of bases for the allosteric strategy.

## Real-time fluorescence analysis of time response characteristics of allosteric strategies

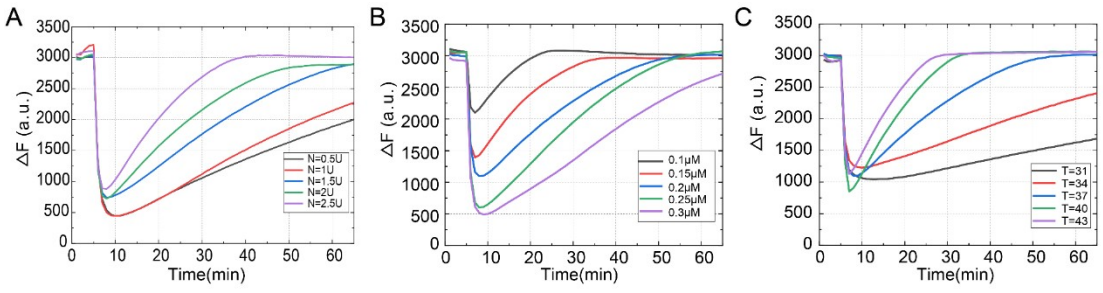

Figure S3. (A) Fluorescence analysis of the structure S automatically reset to its initial state at different enzyme concentrations. (B) Fluorescence analysis of the structure S automatically reset to its initial state at different fuel strand concentrations. (C) Fluorescence analysis of the structure S automatically reset to its initial state at different temperatures. ([D] = 0.2 μM, Nb.BtsI = 2 U, T=37 ℃).

## S3. Design of the DNA switch with self-resetting function

## Design of the DNA switch input signal

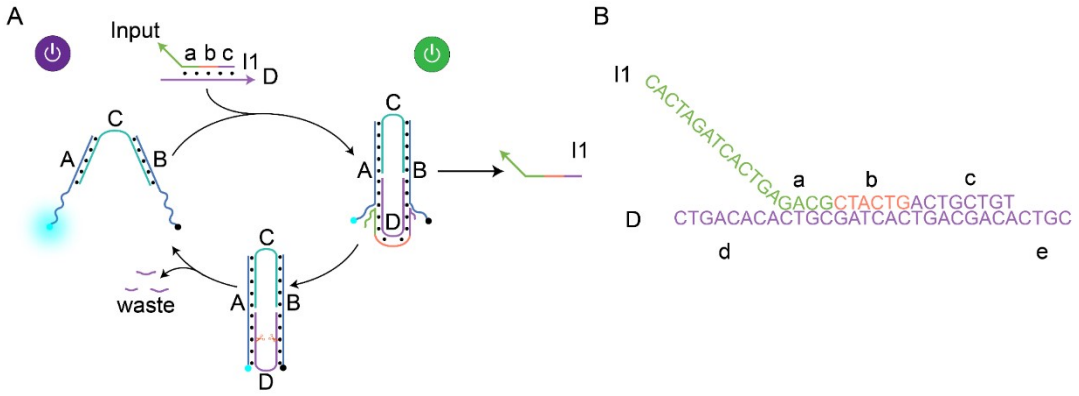


Figure S4. (A) Diagram of the DNA switch with self-resetting function. (B) Diagram of the input signal design.

To verify the scalability of allosteric strategies, we constructed a DNA switch with a self-resetting function, as shown in Figure S4A. In this design, the DNA switch received the input signal to generate the output signal and returned to the initial state. As shown in Figure S4B, the input signal consisted of a double-stranded structure formed by strands D and I1, where domains d and e in strand D served as toeholds for strand displacement reactions. By designing the base sequence of domain b, we could realize the programmable control of the downstream reaction path.

## PAGE analysis of the self-resetting function of the DNA switch

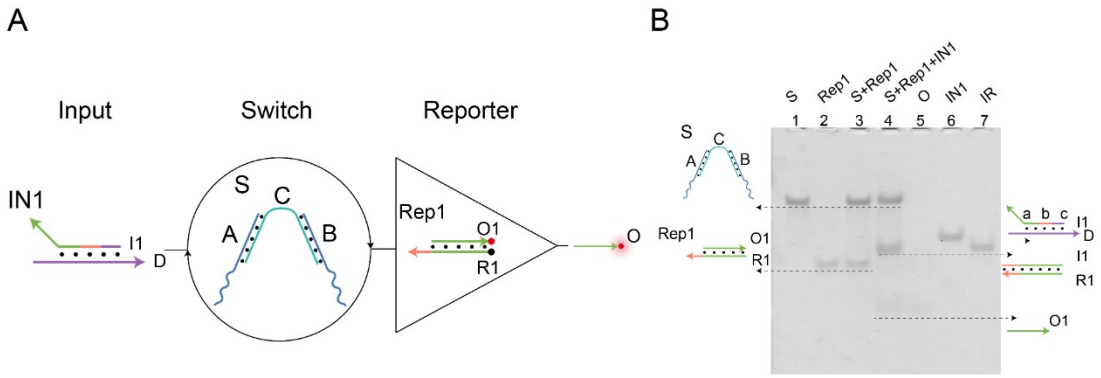


Figure S5. (A) Abstract diagram of DNA switch with self-resetting function. (B) PAGE analysis of self-resetting DNA switches. The input and substrate of each lane are marked at the top of the gel. ([S] = [Rep] = 1 μM, [IN1] = 2 μM, Nb.BtsI = 2.5 U).

To demonstrate the self-resetting function of the DNA switch, we analyzed the

PAGE experiment, and the experimental results are shown in Figure S5B. When there was no input signal, the switch and the Rep1 did not undergo a reaction (lane 3). When the signal was input, the downstream signal strand I was released and reacted with the Rep1 to produce strand O. The switch state changed from "S-ON" to "S-OFF" and autonomously reset to the initial state "S-ON" under the action of the enzyme (lane 4).

## Real-time fluorescence analysis of output signals with different concentration ratio of the input to the substrate

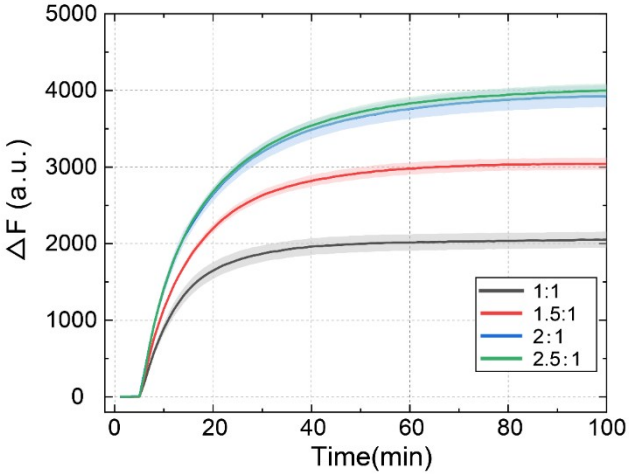


Figure S6. Fluorescence kinetic analysis of output signals with different concentration ratio of the input to the substrate. ([Rep1] = [S] = 0.2 μM, Nb.BtsI = 1 U). The fluorescence values were averaged across the three experiments.

## Real-time fluorescence analysis of output signals under different combinations of input strand concentrations and enzyme concentrations

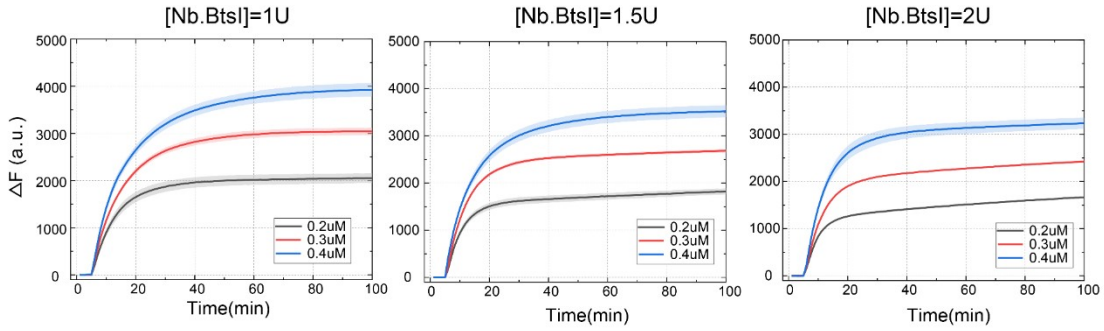


Figure S7. Fluorescence kinetic analysis of output signals of self-resetting switches with different input strands concentration and enzyme concentration combinations. The fluorescence values were averaged across the three experiments.

## S4. Fan-out and fan-in of self-resetting DNA switching circuits

## Fan-out of self-resetting DNA switching circuits

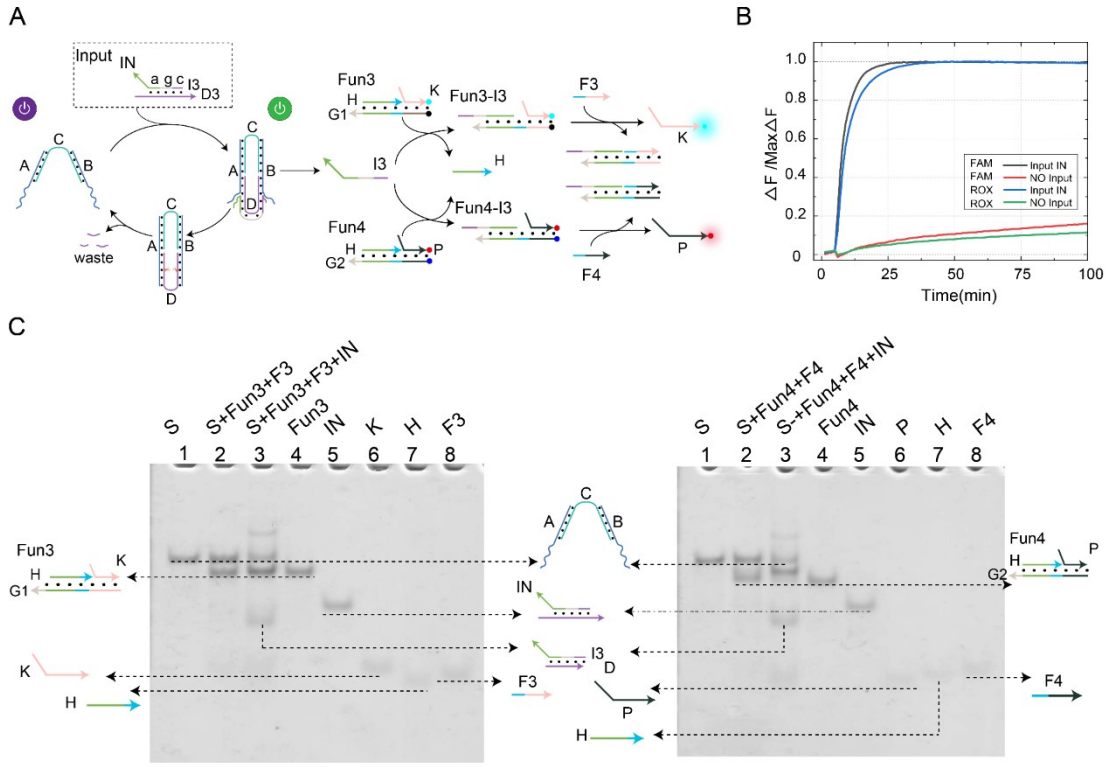


Figure S8. Fan-out function of the self-resetting DNA switching circuits. (A) Schematic diagram of the fan-out function. (B) Real-time fluorescence analysis of the fan-in function. ([S] = [Fun3] = [Fun4] = [F3] = [F4] = 0.2 μM, [IN] = 0.8 μM, Nb.BtsI = 1 U). The fluorescence values were averaged across the three experiments. (C) Polyacrylamide gel electrophoresis analysis of fan-out function. The input and substrate of each lane are marked at the top of the gel. ([S] = [Fun3] = [Fun4] = [F3] = [F4] = 1 μM, [IN] = 2 μM, Nb.BtsI = 2.5 U).

Figure S8 demonstrates the fan-out functionality of the self-resetting DNA switching circuits. The reaction process of the fan-out function is shown in Figure S8A. Firstly, the feasibility was verified through the PAGE experiment. As shown in Figure S8C, Lanes 1, 4, 5, 6, 7, and 8 are reference substances, in which we added only S, Fun3/Fun4, IN, K/P, H, and F3/F4, respectively. In the absence of input IN, no reaction was observed between the functional substrates Fun3/Fun4, switch structure S, and the fuel strand F3/F4 (lane 2). When the input IN was present, apparent strands K and P were generated (lane 3). This experimental result demonstrated that a single input signal IN generated two distinct output signals K and P. Secondly, the fan-out function of the switching circuit was further verified by real-time fluorescence experiments, as shown in Figure S8B. In the absence of input IN, no significant fluorescence signal was observed. When the input IN was present, FAM and ROX output signals increased significantly. The above experimental results were consistent with the PAGE

experiment, confirming the feasibility of the fan-out function of self-resetting DNA switching circuits.

## Specificity of self-resetting DNA switching circuits

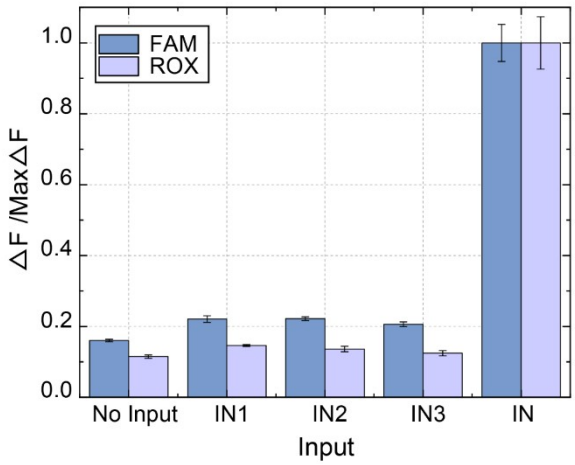


Figure S9. Fluorescence histogram analysis of the specificity of the self-resetting DNA switching circuit with fan-out function. ([S] = [Fun3] = [Fun4] = [F3] = [F4] = 0.2 μM, [IN] = [IN1] = [IN2] = [IN3] = 0.8 μM, Nb.BtsI = 1 U). The fluorescence values were averaged across the three experiments.

## Fan-in of self-resetting DNA switching circuits

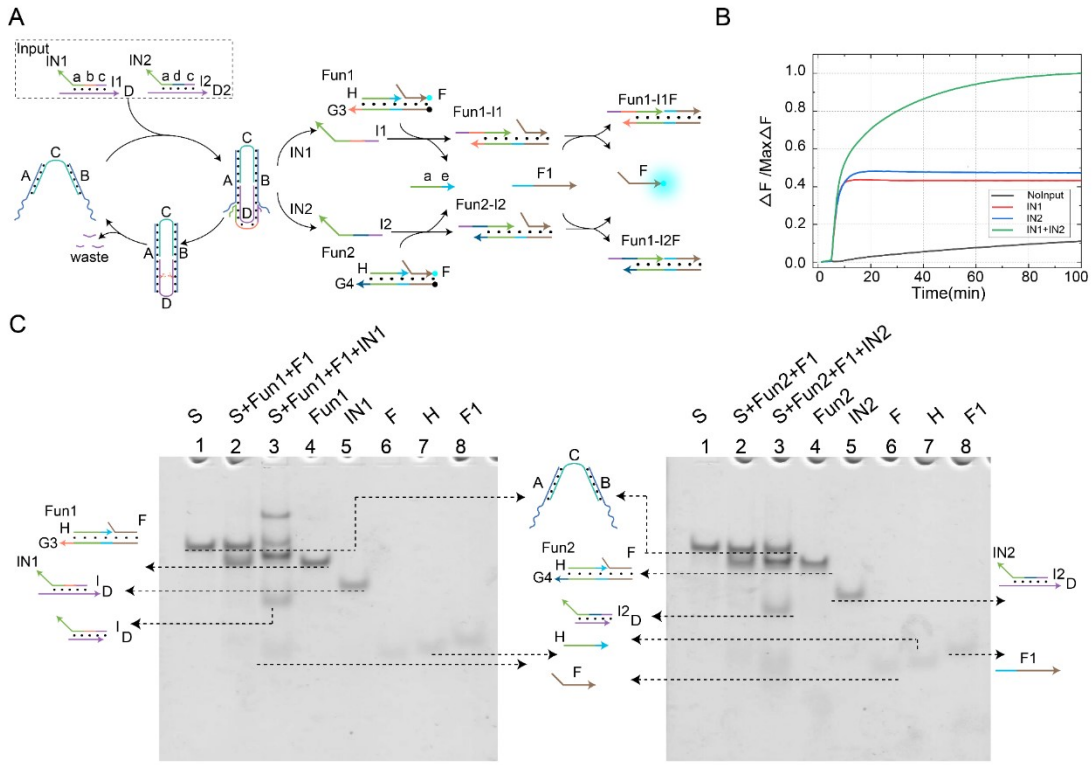


Figure S10. Fan-in function of the self-resetting DNA switching circuits. (A) Schematic diagram of the fan-in function. (B) Real-time fluorescence analysis of the fan-in function. ([S] = [Fun1] =

[Fun2] = 0.2 μM, [IN1] = [IN2] = [F1] = 0.4 μM, Nb.BtsI = 1 U). The fluorescence values were averaged across the three experiments. (C) Polyacrylamide gel electrophoresis analysis of fan-in function. The input and substrate of each lane are marked at the top of the gel. ([S] = [Fun1] = [Fun2] = [F1] = 1 μM, [IN1] = [IN2] = 2 μM, Nb.BtsI = 2.5 U).

Figure S10 shows the implementation of the fan-in function of the self-resetting DNA switching circuits. The reaction process of the fan-in function is shown in Figure S10A. Firstly, we conducted gel electrophoresis experiments for analysis, as shown in Figure S10C. Lanes 1, 4, 5, 6, 7, and 8 are reference substances, in which we added only S, Fun1/Fun2, IN1/IN2, F, H, and F1, respectively. Both lanes 2 and 3 contain S, Fun1/Fun2, and F1; the difference is that IN1/IN2 was added to lane 3. Compared with lane 2, in lane 3, we observed the appearance of strand F in both gel lanes. This shows the feasibility of the fan-in function of the switching circuits. Secondly, by observing real-time fluorescence traces, we noticed that the fluorescence yield in the presence of only one input signal was about half that in the presence of two input signals, as shown in Figure S10B. This observation was consistent with the results from the PAGE experiment, confirming the successful implementation of the fan-in function in the self-resetting DNA switching circuits.

## S5. A parallel DNA switching circuit for complex information processing

## Recognition module

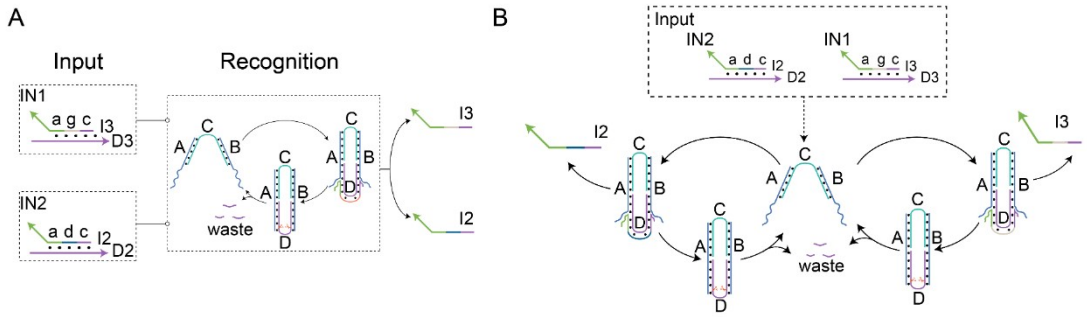


Figure S11. (A) Abstract diagram of the reaction process in the recognition module. (B) Schematic diagram of the reaction process in the recognition module.

## Translation module

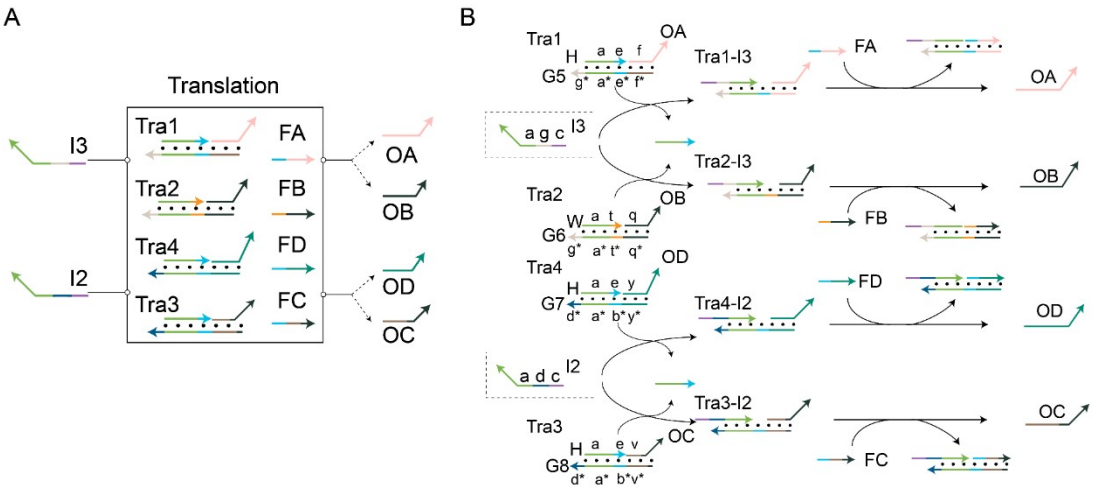


Figure S12. (A) Abstract diagram of the reaction process in the translation module. (B) Schematic diagram of the reaction process in the translation module.

## Decision module

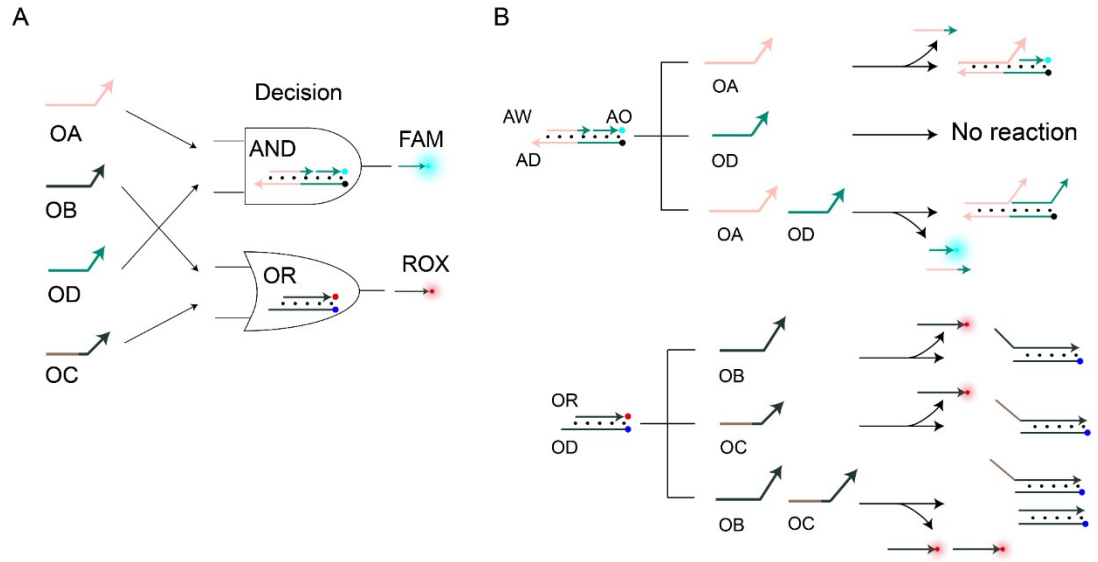


Figure S13. (A) Abstract diagram of the reaction process in the decision module. (B) Schematic diagram of the reaction process in the decision module.

## Real-time fluorescence analysis by parallel AND and OR logic operations

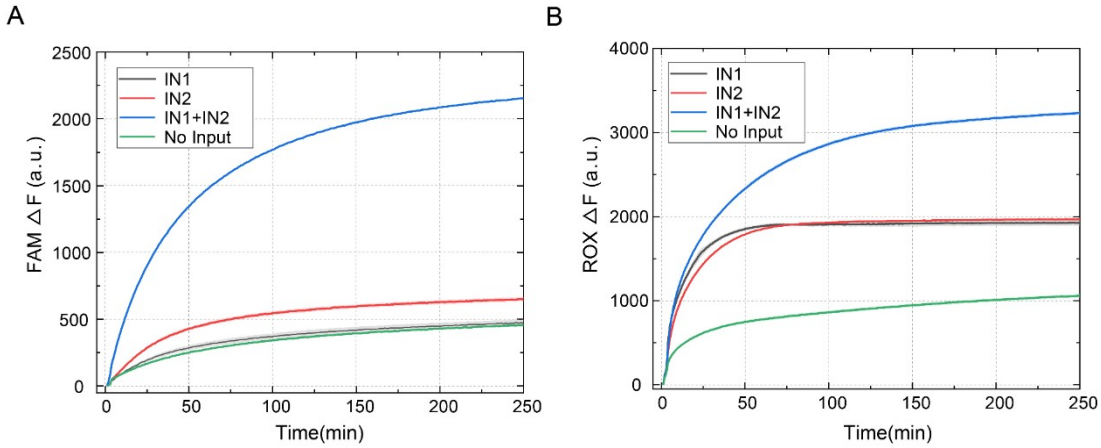


Figure S14. Fluorescence analysis of AND and OR parallel logic operations. (A) Fluorescence analysis of AND logic operations. (B) Fluorescence analysis of OR logic operations. The fluorescence values were averaged across the three experiments.

## Implementation of logic operations for different input combinations

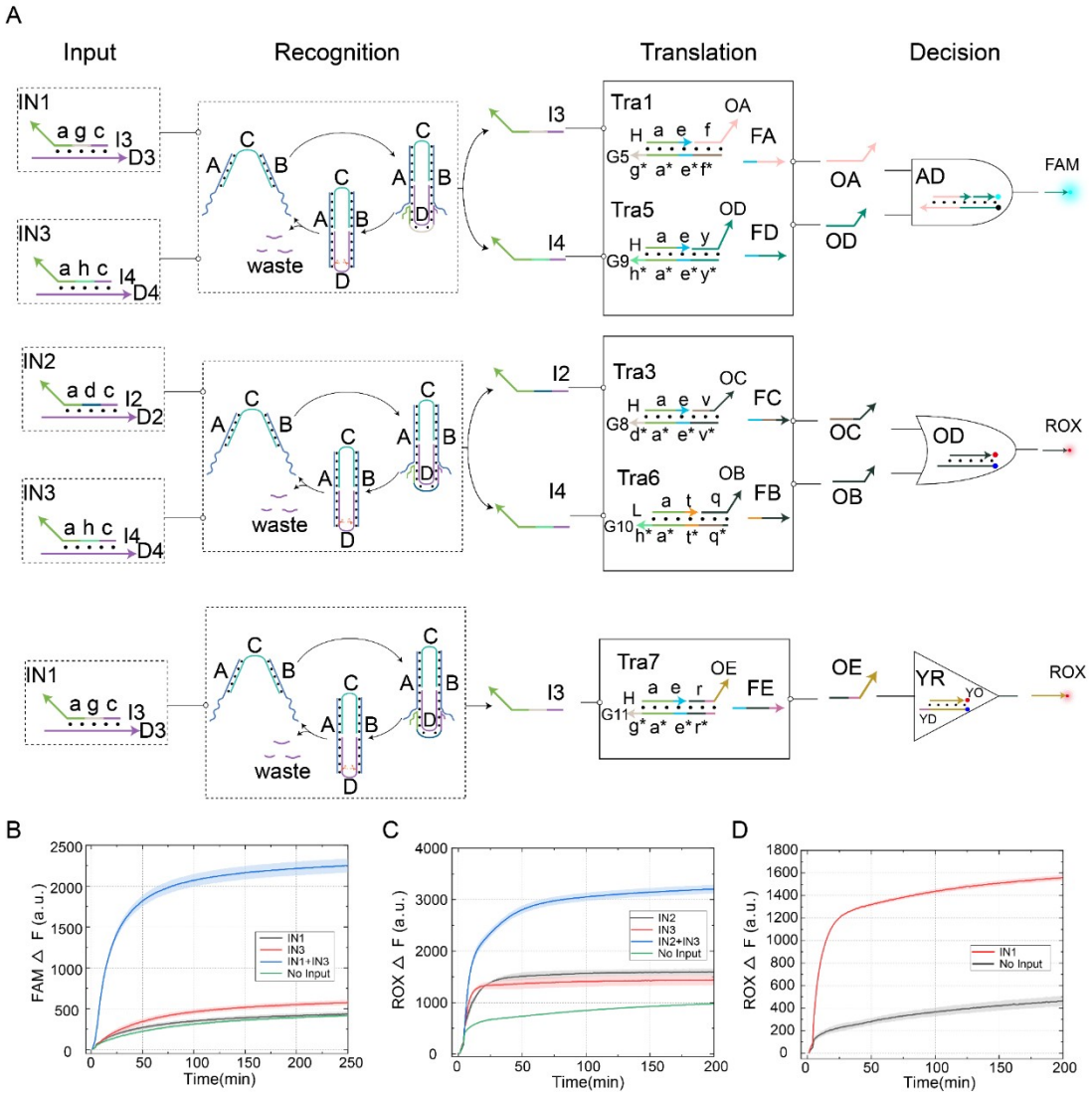


Figure S15. (A) Diagram of logical operation under different input combinations. (B) Fluorescence analysis of AND logic operation. (C) Fluorescence analysis of OR logic operation. (D) Fluorescence analysis of YES logic operation. ([S] = 0.1μM, [Tra1] = [Tra3] = [Tra5] = [Tra6] = [Tra7] = 0.1 μM, [FA] = [FB] = [FC] = [FD] = [FE] = 0.1 μM, [IN1] = [IN2] = [IN3] = 0.2 μM, [AD] = [OD] = [YD] = 0.1 μM, Nb.BtsI = 1 U). The fluorescence values were averaged across the three experiments.

As shown in Figure S15A, when we changed the input combination, the self-resetting DNA switching circuits could still receive different input signals to achieve complex logic operations, proving the circuit's multi-information processing capability. This was further verified by real-time fluorescence analysis. In Figure S15B, the self-resetting DNA switch circuit successfully performed the AND logic operation by inputting IN1 and IN3. In Figure S15C, the circuit achieved the OR logic operation by inputting IN2 and IN3. In Figure S15D, the YES logic operation was accomplished by inputting IN1 alone.